Materials Today Chemistry 34 (2023) 101783

Contents lists available at ScienceDirect

Materials Today Chemistry

journal homepage: www.journals.elsevier.com/materials-today-chemistry/

# Single-electron transfer reactions on surface-modified gold plasmons

Robert Bericat-Vadell [a,1], Pandiaraj Sekar [a,1], Yeersen Patehebieke [b], Xianshao Zou [a], Nidhi Kaul [a], Peter Broqvist [c], Rebecka Lindblad [d], Andreas Lindblad [d], Anna Arkhypchuk [e], Carl-Johan Walletin [b,**], Jacinto Sá [a,f,*]

[a] Physical Chemistry Division, Department of Chemistry - Angstrom Laboratory, Uppsala University, 751 20, Uppsala, Sweden
[b] Department of Chemistry and Molecular Biology, University of Gothenburg, Kemivägen 10, 412 58, Gothenburg, Sweden
[c] Structural Chemistry Division, Department of Chemistry - Angstrom Laboratory, Uppsala University, 751 20, Uppsala, Sweden
[d] X-ray Photon Science, Department of Physics and Astronomy, Uppsala University, 751 20, Uppsala, Sweden
[e] Synthetic Molecular Chemistry, Department of Chemistry - Angstrom Laboratory, Uppsala University, 751 20, Uppsala, Sweden
[f] Institute of Physical Chemistry, Polish Academy of Sciences, Marcina Kasprzaka 44/52, 01-224, Warsaw, Poland

A B S T R A C T

Photoredox catalysis's relevance in organic synthesis research and innovation will increase in the coming decades. However, the processes rely almost exclusively on expensive noble metal complexes, most notably iridium complexes, to absorb light and transfer a single charge to a substrate or a catalyst to initiate cascade transformations. Light-triggered plasmon resonances generate a non-Fermi-Dirac energy distribution with many hot carriers that decay in ~1 ps. Their ultrafast relaxation makes performing single electron transfer (SET) transformations challenging. Herein, a novel photosystem is proposed based on surface-modified gold nanoparticles (aka *plasmon "molecularization"*), which improved charge separation and, more importantly, enabled SET reactions, expanding the portfolio of photocatalysts available for photoredox catalysis. The photosystem was made into an electrode, permitting its use in photoelectrochemical arrangements that leverage electro- and photo-chemical approaches' benefits and chemical engineering solutions, helping the synthetic chemistry efforts towards greener synthesis and synthesis of more complex structures on a scale.

## 1. Introduction

Chemistry and its industry contribute to almost every part of modern life, producing fuels, bulk chemicals, polymers, fine chemicals and pharmaceuticals [1]. It is fair to say that the chemical industry improved living standards by increasing food supply, nutrition, sanitation, and medications. While these positive contributions to the quality of life can be recognised, the chemical industry and its manufacturing operations are directly responsible for Earth's natural resources decline and significant greenhouse gas emissions [2]. The rise of globalised supply chains that have enabled the chemical industry to source materials and precursors from suppliers in developing nations drove down the price of products. It has also influenced consumer behaviour, promoting a "throw-away" culture with immeasurable social, environmental, and economic costs. It is incumbent on scientists and engineers to develop novel synthetic routes and chemical processes to manufacture chemicals in line with the UN sustainability goals.

Photoredox catalysis is a class of chemical transformations in which photoactive catalysts, typically a noble metal complex, such as iridium or ruthenium complexes, generate electrical charges (electrons and holes) upon light absorption, which are subsequently transferred to a substrate or catalyst that initiates cascade reactions [3–5]. Photoredox catalysis is a relatively new approach in organic synthesis but has shown great aptitude in developing more sustainable and efficient chemical synthesis methods [6]. However, their overreliance on expensive noble metal complexes limits reaction engineering and complicates workflows that separate them from the reaction medium. Heterogenisation is a possibility [7], but it often affects catalytic performance and is prone to catalyst leaching. One needs disruptive new ways to initiate these transformations to maximise photoredox catalysis potential.

Plasmons are highly effective materials for light absorption and hot carrier generation, which is why they have been applied to photocatalysis [8–19]. The excitation of its localised surface plasmon resonance creates a non-thermal distribution of multiple carriers that could be harnessed for chemical reactions [20,21]. However, multi-charge makes its adaptation to photoredox catalysis difficult because, in

* Corresponding author.
** Corresponding author.
*E-mail addresses:* carl.wallentin@chem.gu.se (C.-J. Walletin), jacinto.sa@kemi.uu.se (J. Sá).
[1] equal contribution.

https://doi.org/10.1016/j.mtchem.2023.101783
Received 30 August 2023; Received in revised form 9 October 2023; Accepted 18 October 2023
Available online 3 November 2023

photoredox catalysis, single electron transfer (SET) is the primary mechanism of the reaction [22–24]. The fact is exacerbated by the ultrafast relaxation of the carriers (~1 ps), which left questions about their involvement in the photocatalytic process [25,26]. This is a fair remark since most of the reported plasmon photocatalysis could be equally catalysed by the photothermal process, which is inescapably present.

SET is a chemical reaction in which an electron is transferred from one molecule (the electron donor) to another molecule (the electron acceptor) in a single step, often a system consisting of a photosensitiser and a substrate or catalyst. This process typically occurs through intermediate steps involving forming transient species, such as radicals. The rate of SET reactions is governed by the energy difference between the donor and acceptor drives electron transfer (Marcus's theory) [27]. According to Marcus's theory, the rate of an electron transfer reaction depends on the electronic coupling between the donor and acceptor, the reorganisation of the solvent and the energy difference between the donor and acceptor. Examples include biological systems, e.g., enzyme-catalysed reactions, photosynthesis and respiration, and inorganic systems, e.g., electrochemical cells and solar energy conversion [28–36]. Importantly, these processes occur at moderate temperatures and involve single electrical charges, challenging for plasmonic materials due to multiple charges and their ultrafast relaxations.

Herein, a strategy to transform Au plasmonic into a SET photocatalyst is proposed. Surface modification with thiophenols enabled SET chemical reactions in solid electrodes. Crucially, the provenience of the carriers could be traced to the plasmon resonance decay by ultrafast infrared spectroscopy. The findings establish plasmons as a viable photosensitiser/-catalyst for photoredox catalysis. They keep their inherent advantages, such as strong light absorption, chemical stability and extensive redox window, while offering easy design and tunability by simple ligand surface modification.

## 2. Results & discussion

Materials synthesis and electrode manufacturing are described in supporting information (SI). The Au colloidal nanoparticles (Au NPs) were prepared using a modified version of the modified Turkevich method [37]. Dynamic light scattering (DLS) analysis has a single feature centred at 8 ± 2 nm, confirming sample homogeneity regarding particle size distribution (Fig. S1), which was also substainciated by atomic force microscopy (Fig. S2). The Au NPs have an optical plasmonic peak at 515 nm, which shifted to 550 nm when deposited on fluorinated tin oxide (FTO) glass (Fig. S3). Adding thiophenols (modifiers) did not significantly change the absorption peak position (Fig. S3). Deposition of the Au NPs on $TiO_2$ shifted further the absorption to about 580–590 nm due to changes in the dielectric surrounding. Note that the capping agent (citrate) is completely removed after the annealing step, as confirmed by infrared measurements.

X-ray photoelectron spectroscopy (XPS) survey analysis was used to establish the Au relative abundance (Figs. S4 and S5). Looking at the relative intensity of the Ti *2p* and Au *4f* peaks, it is clear that the samples are relatively homogeneous in Au abundance. Thus, differences in

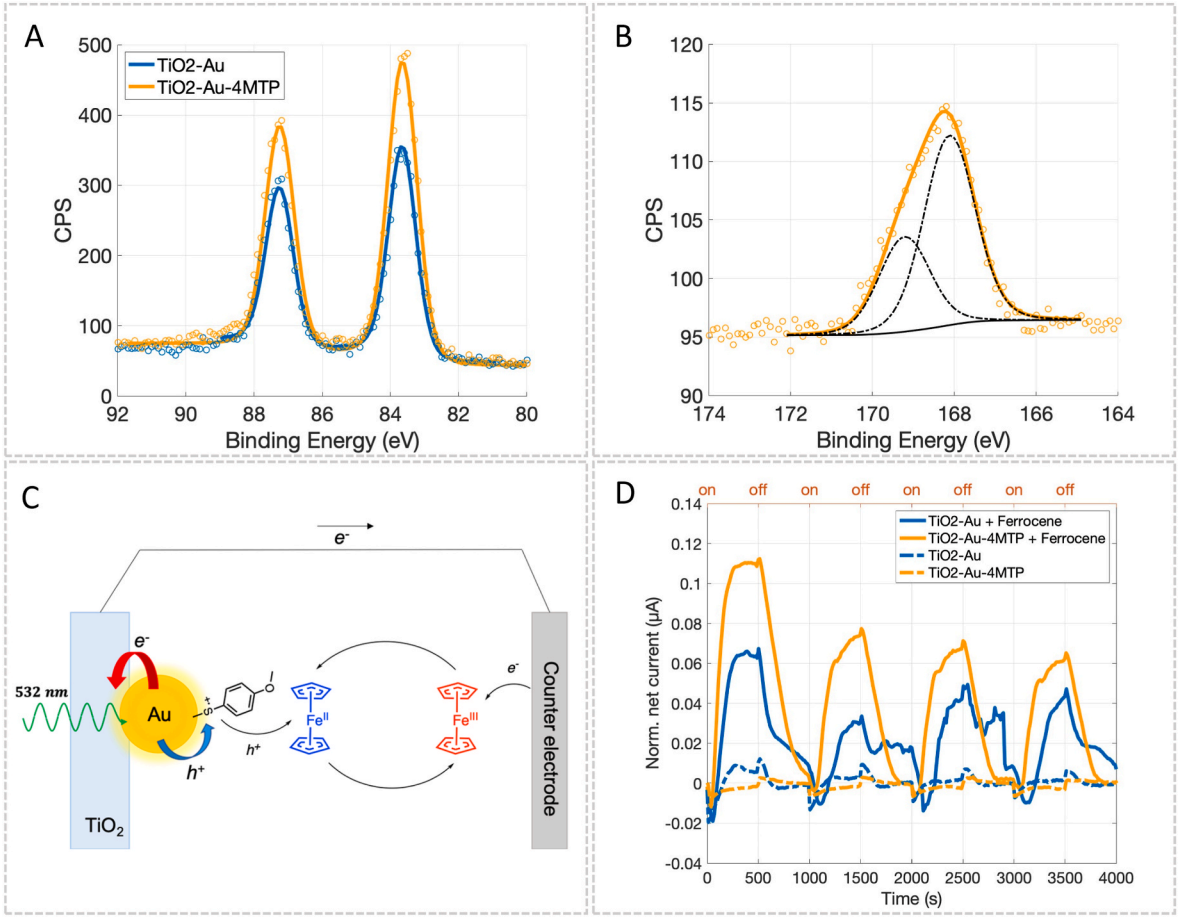


**Fig. 1. Surface modification and effect on ferrocene reversible SET reaction.** A) XPS Au *4f* region of $TiO_2$/Au without modification (TiO2–Au) and modified with 4-methoxy thiophenol (TiO2–Au-4MPT); B) XPS S *2p* region of $TiO_2$/Au modified with 4-methoxy thiophenol (TiO2–Au-4MPT); C) Reaction scheme depicting the reversible photo-oxidation of ferrocene with $TiO_2$/Au electrodes with 4-methoxy thiophenol modification; and D) In situ chronoamperometry studies of the reversible ferrocene oxidation with 0.1 V vs $Ag/Ag^+$ ion non aqueous reference electrode, depicting the effect of surface modification. (on) under 532 nm CW laser illumination; and (off) without light.

catalytic output are unrelated to the samples' gold content. Fig. 1A shows the XPS narrow scan region of Au *4f* of $TiO_2$/Au pristine (TiO2–Au) and modified with 4-methoxy thiophenol (TiO2–Au-4MPT). In the absence of thiphenol the Au *4f* was fitted with a single doublet and had an Au $4f_{7/2}$ with a binding energy of 83.7 eV, which is consistent with gold in metallic form [38,39]. The addition of the thiophenol did not change the gold fitting or binding energy. The S *2p* of the modified sample is presented in Fig. 1B. The signal was fitted with a single doublet with an S $2p_{3/2}$ at 168 eV. Note that thiophenol modification of Au occurs with a formation of an Au–S bond [40]. The Au–S bond from thiol modification of gold surfaces yields an S $2p_{3/2}$ peak at 162 eV [41], in which the sulfur is not donating electron density to the gold. An additional small peak at 164 eV is occasionally observed due to unbound sulfur on the surface [42,43]. However, in the present case, a single feature at high binding energy was detected that did not change in intensity after sample washing. According to XPS O 1s signal (Fig. S6), there is also no evidence of sulfur oxidation, which is dominated by a single peak from the $TiO_2$ semiconductor. Therefore, this is a bonded sulfur with a higher binding energy, suggesting a significant electron donation to the Au nanoparticles.

The reversible ferrocene oxidation is a common SET reaction with an $Fc/Fc^+$ oxidation potential of +0.31 V vs SCE [44,45]. According to Roth et al., the potential is within the oxidation window of the thiophenol modifiers (Fig. S7) [46]. Fig. 1C shows a schematic representation of the reaction and the electrodes used to evaluate the effect of gold-surface modifications. Briefly, the excitation of the gold plasmon resonance results in the formation of hot electrons and holes. The electrons are transferred to the $TiO_2$ (electron acceptor) and the holes to the thiophenol (hole acceptor), which in the figure is represented by the 4-methoxythiophenol. Once there, the hole can react with the ferrocene oxidising it. The electron is sent across the electrochemical cell and reacts with the oxidised ferrocene molecule at the counter electrode. There is also the possibility that the hot hole reacts directly with the ferrocene on the Au surface, which is why the activity is compared to the unmodified system. Monitoring of the photoelectrochemical current provides direct information on system activity.

Fig. 1D compares the activities of $TiO_2$/Au without modification (TiO2–Au) and modified with 4-methoxy thiophenol (TiO2–Au-4MPT) in the absence and presence of ferrocene and light. Both systems showed very small photocurrents when ferrocene was absent, thus confirming that the measured photocurrent relates to the ferrocene oxidation reaction. No current was detected when the light was absent (not shown). In the presence of ferrocene, both systems showed measurable amounts of photocurrent, with the system modified with 4-methoxy thiophenol showing ~ 4–5 times more photocurrent. From XPS analysis, it is possible to exclude the possibility that the changes in activity are related to differences in the amount of gold. Therefore, the increased photocurrent indicates a constructive role of surface modification in the catalytic output. Note that despite the absence of electrolyte and active stirring, the current responds to light modulation promptly, supporting the involvement of hot electrons rather than a photothermal-mediated reaction [47]. Moreover, the gold loading is comparable, meaning one can expect a similar contribution (if any) of the photothermal process in the conversion for both samples. Thus, the difference in activity cannot be related to it. Finally, it is worth pointing out that ferrocene has relatively low thermal stability decomposing at temperatures between 450 and 500 K [48], which are insufficient to perform the oxidation reaction from an energetic perspective.

The adaptability and versatility of the approach were evaluated using two additional thiophenols, namely naphthalene thiophenol and thiophenol, which have an oxidation potential of 1.33 V vs standard calomel electrode (SCE) and 1.51 V vs SCE, respectively that is higher than the 4-methoxy thiophenol (1.15 V vs SCE) (Fig. S6). Despite being prepared using the same methodology and having the same anchoring group (i.e., S–H), the loading was significantly different for reasons that are not 100 % clear. Therefore, to compare catalytic activity, the chronoamperometry was normalised by the XPS area ratio of S *2p* and Au $4f_{7/2}$ (Table S1). The normalised chronoamperometry data is shown in Fig. S8. All modifications positively affected the measured photocurrent, demonstrating the approach's adaptability.

The normalised integrated photocurrent was plotted versus the oxidation potential (Fig. S9) to evaluate if there is any trend. The data reveals a volcano shape with an optimum obtained with naphthalene thiophenol. The reaction occurs via the collision of the substrate with the thiophenol, which should not be affected significantly by the molecule structure. Therefore, the findings relate to changes in oxidation potential (i.e., changes in reaction driving force according to Marcus' theory) [21] and the amount of charge available. As the oxidation potential of the modifier increases, the rate increases since the driving force increases. However, the hot carriers follow a Boltzmann energy distribution. Thus, at some point, the population of carriers with sufficient oxidation potential becomes limiting, meaning fewer modifiers are oxidised. Consequently, there is a drop in activity, as seen with thiophenol. Note that this is a preliminary analysis of the modifier effect, and further studies need to be performed to validate this hypothesis, which is beyond the scope of the work.

To substantiate the involvement of the hot electrons in the process, ultrafast transient infrared absorption spectroscopy (TIRAS) experiments were conducted. TIRAS experiments were performed, exciting the Au-plasmon resonance on the red of the absorption peak (550 nm) to capture related solely to the plasmon component, i.e., avoid intraband unravel contributions to the signal [49,50]. The TIRAS colour maps (Fig. 2A and S10) are dominated by a broad featureless absorption, characteristic of forming a quasi-metallic state due to free carriers [51,52]. Fig. 2B shows the kinetic traces extracted at 5200 nm (1923 $cm^{-1}$) for data normalised to the highest intensity. Both systems showed characteristic signals associated with electron injection into $TiO_2$ prevenient from the Au plasmon. The injection occurs within the instrument function resolution (~300 fs). It is also noticeable that most of the charge recombines too quickly to be useful for catalysis. Still, a small population of charge surviving beyond 1 ns (≥2 %) would accumulate under continuous illumination (reaction conditions), making them beneficial to drive the photocatalytic process. Finally, from a simple visual inspection, adding 4-methoxy thiophenol positively affects the charge separation state lifetime.

Kinetic trace decays were fitted with three exponential decays. The shorter decay relates to interfacial recombination shortly after injection, and the second and third decays to bulk recombination. For the $TiO_2$/Au system, the fitted time components were $\tau_1 = 0.11 \pm 0.10$ ps (95 %), $\tau_2 = 1.7 \pm 0.2$ ps (3.8 %) and $\tau_3 = 52.7 \pm 14$ ps (1.2 %), while for the $TiO_2$/Au modified with 4-methoxy thiophenol, they were $\tau_1 = 1.32 \pm 0.19$ ps (66 %), $\tau_2 = 13.3 \pm 4.4$ ps (21 %) and $\tau_3 = 285 \pm 14$ ps (13 %). The addition of the 4-methoxy thiophenol dramatically increases the lifetime of the system, in particular, the longed lived charge, where both time and percentage of amount surviving increase significantly.

Fig. 2C shows the TIRAS kinetic trace for the unnormalised data at a short time range. It is perceptible that the signal intensity around time zero is smaller for the modified system than the pristine $TiO_2$/Au. To interpret this difference, one must establish if electrons on $TiO_2$ are the sole corporate for the observed 'free carrier' signal and if there is evidence for the sulfur oxidation. Tight-binding computational calculations using the semiempirical GFN2-xTB model [53] indicate that hole transfer to the thiophenols with a hole localisation at the sulfur atom should change the absorption peaks (Figs. S11–S13). However, TIRAS measurements performed in the region of interest (2900-3100 $cm^{-1}$) did not yield measurable changes in the signal even when the experiments were carried out with Au NPs and modifiers without the $TiO_2$. The Au-4-methoxy thiophenol sample showed a signal resembling the 'free carrier', namely broad featureless absorption across the entire mid-infrared region (Fig. 2D). The kinetic traces of the normalised signal extracted at 5200 nm comparing Au and Au-modified 4-methoxy thiophenol is shown in Fig. S14 and reveals a longer-lived signal when the

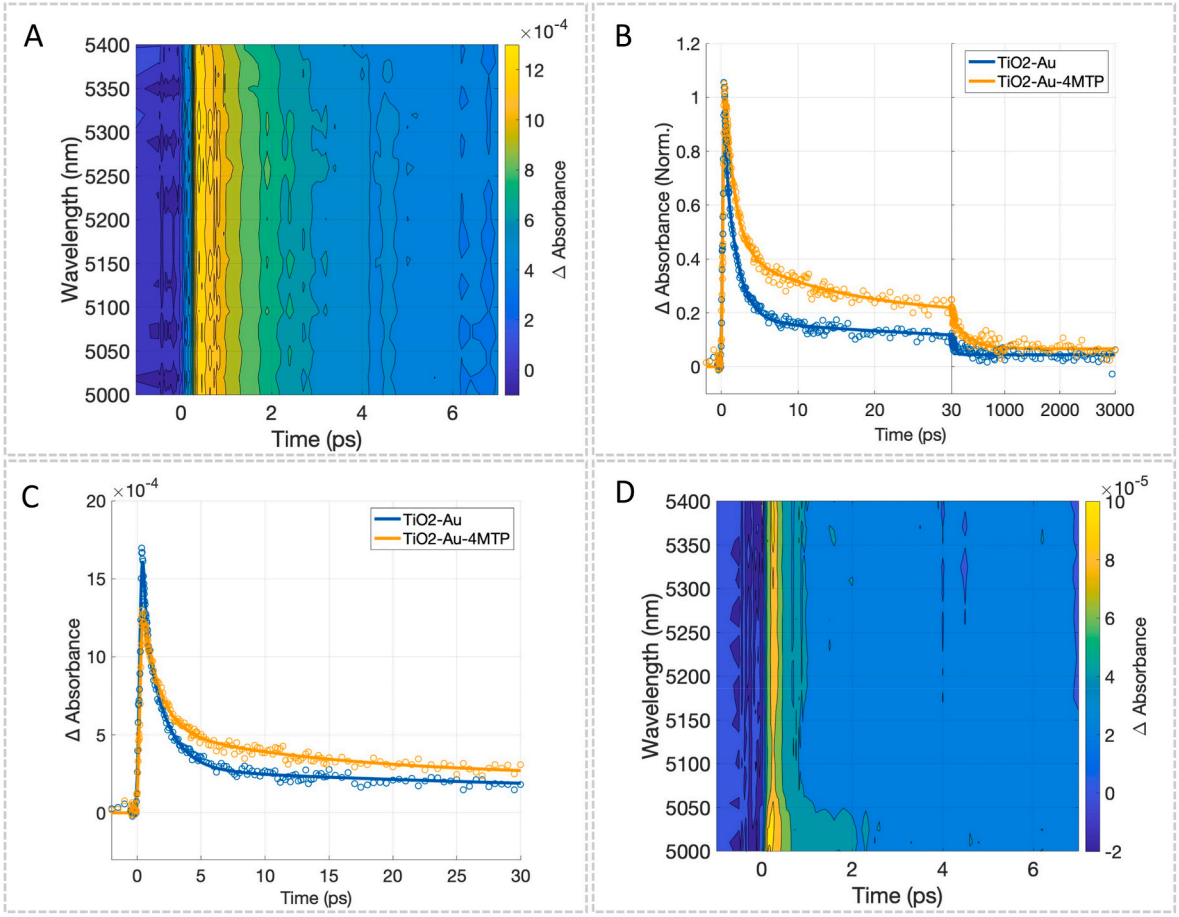


**Fig. 2. TIRAS measurements depicting hot carriers transfer after Au-plasmon excitation at 550 nm.** A) colour map of the sample $TiO_2$/Au modified with 4-methoxy thiophenol; B) kinetic traces of the normalised data extracted at 5200 nm over the entire delay line; C) kinetic traces of the unnormalised data extracted at 5200 nm at shorter times; and D) colour map of Au-4-methoxy thiophenol after Au-plasmon excitation at 550 nm. (For interpretation of the references to colour in this figure legend, the reader is referred to the Web version of this article.)

modifier is present. This indicates that the modifier contributes to the signal related to Au transient absorption due to laser-induced conductivity changes. The observation suggests that Au-thiophenol assemble 'shares' the hole, i.e., the hole is not localised at the sulfur, which is expected for strong plasmon-molecular coupling systems [54]. The strong coupling was aforementioned when presenting the XPS analysis.

While this explains the shape of the signal observed when $TiO_2$ is absent, it makes the decrease in signal amplitude even more puzzling since, in the modified samples, two species are contributing to the free carrier signal. Thus, one would expect a higher signal amplitude. Recently, we demonstrated that hot hole injection effectively decreases the average temperature of the electrons [55], i.e., the number of hot electrons with sufficient energy to overcome the Au–$TiO_2$ Schottky barrier (~1.0 eV).34 Therefore, the result indicates that the hot holes are efficiently transferred to the thiophenol before the hot electrons are injected into the $TiO_2$. Because of that, the electrons' average temperature in the resonance decreases, decreasing the number of injectable electrons. Further support for this hypothesis is that the signal amplitude changes relate to the amount of thiophenol on the surface, meaning hot holes saturate the available ligands quickly; hence their concentration regulates the average electron temperature in the resonance.

The reversible oxidation of ferrocene provided support that surface modification of plasmons unlocks the possibility of doing SET transformations. However, the transformation is simple and without synthetic value. Direct aminooxygenation of alkenes provides straightforward and efficient access to the 1,2-aminoalcohol motif in various bioactive molecules, natural products, and chiral reagents [56–59]. Xu et al.60 developed an electrochemical protocol for the intramolecular aminooxygenation of unactivated alkenes. The process involves the addition of nitrogen-centred radicals, generated through electrochemical oxidation, to alkenes, followed by trapping of the cyclised radical intermediate with 2,2,6,6-tetramethylpiperidine-N-oxyl radical (TEMPO) with a constant 10 mA current, reticulated vitreous carbon (RVC) anode and a platinum wire cathode. By replacing the RVC anode with the $TiO_2$–Au system modified with 4-methoxy thiophenol photoanode, it was possible to validate the applicability of the proposed photosystem in synthetically relevant transformations. 3-Methylbut-2-enyl phenylcarbamate was used as the substrate, prepared according to Xu et al. [60] reported methodology. The substrate structure was confirmed by $^{1}H$ and $^{13}C$ nuclear magnetic resonance (NMR) (Figs. S14 and S15), matching what has been reported elsewhere [61,62].

Fig. 3A shows the light modulation chronoamperometry data when 3-methylbut-2-enyl phenylcarbamate was used only substrate. The current was only detected in the presence of light, and thus it relates to the photocatalytic process. The photocurrent detected is very low in the absence of TEMPO. With only TEMPO, the detected photocurrent was two orders of magnitude higher (Fig. 3B), confirming the critical role of TEMPO as substrate and co-catalyst. Nevertheless, it is noticeable that the thiophenol-modified photoelectrode had almost double the photocurrent compared to the unmodified, corroborating the findings with the ferrocene experiments.

Fig. 3B shows the light modulation chronoamperometry data with 3-methylbut-2-enyl phenylcarbamate and TEMPO. Once more, it is noticeable that the photoelectrode modification with thiophenol

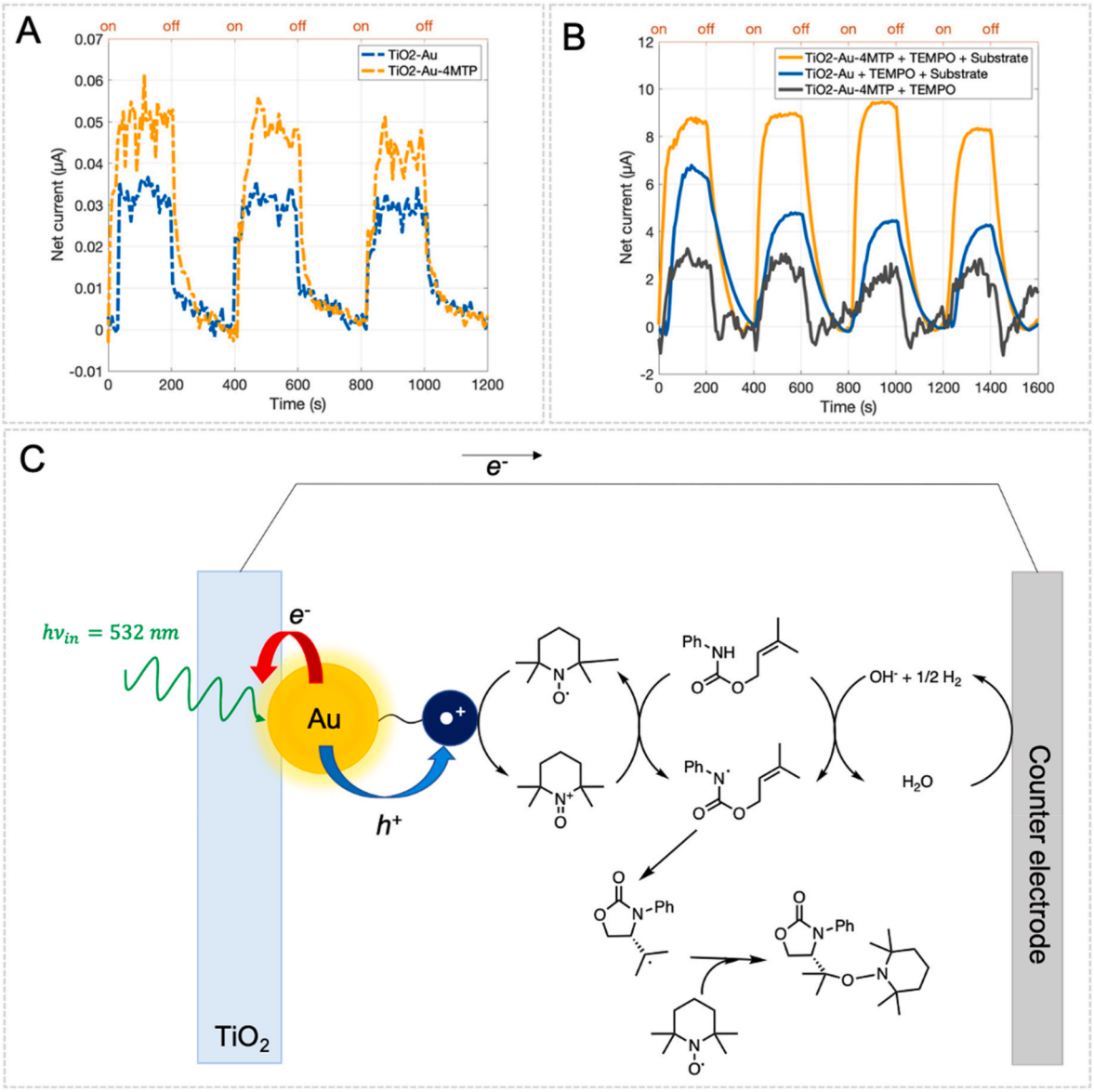


**Fig. 3. Single electron transfer aminooxygenation of unactivated alkenes on $TiO_2$/Au modified with 4-methoxy thiophenol with 0.3 V vs Ag/Ag $^+$ ion non-aqueous reference electrode and 532 nm laser illumination.** A) In situ chronoamperometry data recorded during the catalytic reaction with 3-methylbut-2-enyl phenylcarbamate as the only substrate to establish the role of the thiophenol modification. B) In situ chronoamperometry data recorded during the catalytic reaction revealing the critical role of TEMPO in the reaction; and C) Schematic representation of the reaction mechanism for SET oxidation with 3-Methylbut-2-enyl phenylcarbamate and TEMPO as substrates.

significantly improves the photoelectrocatalytic performance. Reaction performed over 10 h with continuous illumination showed continuous photocurrent (Fig. S16) and yielded a single product. The product was isolated from the reaction crude and identified with $^1$H and $^{13}$C NMR (Figs. S17 and S18). The product spectra matched the one related to 3-phenyl-4-(2-((2,2,6,6-tetramethylpiperidin-1-yl)oxy)propan-2-yl)oxazolidin-2-one [60], the expected reaction product. The average isolated yield of two separate reactions was 87 %.

Fig. 3C illustrates the reaction mechanism, adapted from Xu et al. [60] electrocatalytic process. Light excitation of the plasmon resonance creates a coherent excitation of the valence electrons, which dephases via Landau damping, forming hot electrons and holes. The hot electrons are transferred to the $TiO_2$ semiconductor, consistent with TIRAS and TAS measurements, and react at the counter electrode, leading to hydrogen production and hydroxide ions (base). The hot holes are transferred to the thiophenol modifiers, according to TIRAS and TAS measurements, and subsequently utilised to oxidise TEMPO. The oxidised TEMPO and the hydroxide ions react with the phenylcarbamate alkene substrate, forming a nitrogen-centred radical believed to occur through a concerted proton-coupled electron transfer mechanism. The formed nitrogen-centred radical intermediate cyclises and is quenched by TEMPO to create the final product.

## 3. Conclusion

Thiophenol modifications of plasmonic surface catalysed SET transformations, expanding the photoredox catalysis photocatalyst portfolio and leveraging the unique plasmonic photophysics. The strategy shows that plasmonic materials can be tuned and adapted by carefully selecting surface modifiers to exhibit the correct potentials and charge. The photosystem was made into an electrode, permitting its use in photoelectrochemical arrangements that leverage electro- and photochemical approaches' benefits. The system also provides a more sustainable solution and workflow for photoredox catalysis, liberating it

from its dependence on noble metal complexes that are expensive, unstable and difficult to separate while unlocking the possibility of using chemical engineering solutions to improve catalytic performance and suppress the photoredox catalysis scale-up bottleneck.

## Credit author statement

**Robert Bericat-Vadell**: Conceptualization, Methodology, Data curation, Visualization, Investigation, Writing- Reviewing and Editing, **Pandiaraj Sekar:** Methodology, Data curation, Visualization, Investigation, **Yeersen Patehebieke:** Methodology, Visualization, Investigation, **Xianshao Zou:** Investigation, **Nidhi Kaul:** Investigation, **Peter Broqvist:** Methodology, Investigation, **Rebecka Lindblad:** Methodology, Investigation, **Andreas Lindblad:** Methodology, **Anna Arkhypchuk:** Methodology, **Carl-Johan Walletin:** Conceptualization, Methodology, Data curation, Visualization, Investigation, Writing-Reviewing and Editing, and **Jacinto Sá**: Conceptualization, Methodology, Data curation, Visualization, Investigation, Writing- Original draft preparation.

All authors read agreed with final version of the manuscript.

## Declaration of competing interest

The authors declare that they have no known competing financial interests or personal relationships that could have appeared to influence the work reported in this paper.Jacinto Sa reports financial support was provided by Knut and Alice Wallenberg Foundation. Jacinto Sa reports financial support was provided by Swedish Research Council.

## Data availability

Data will be made available on request.

## Acknowledgements

This project was possible thanks to the support of the Knut & Alice Wallenberg Foundation (grant no. 2019-0071) and the Swedish Research Council (VR) (grant no. 2019-03597).

## Appendix A. Supplementary data

Supplementary data to this article can be found online at https://doi.org/10.1016/j.mtchem.2023.101783.

## References

[1] J. Colberg, K.K. Hii, S.G. Koenig, Importance of green and sustainable chemistry in the chemical industry, ACS Sustain. Chem. Eng. 10 (2022) 8239–8241.
[2] IEA. Chemicals https://www.iea.org/reports/chemicals (accessed 2023-March-23).
[3] D.A. Nicewicz, D.W.C. MacMillan, Merging photoredox catalysis with Organocatalysis: the direct asymmetric Alkylation of Aldehydes, Science 322 (2008) 77–80.
[4] M.A. Ischay, M.E. Anzovino, J. Du, T.P. Yoon, Efficient visible light photocatalysis of [2+2] Enone Cycloadditions, J. Am. Chem. Soc. 130 (2008) 12886–12887.
[5] J.M.R. Narayanam, J.W. Tucker, C.R.J. Stephenson, Electron-transfer photoredox catalysis: develop- ment of a tin- free reductive Dehalogenation reaction, J. Am. Chem. Soc. 131 (2009) 8756–8757.
[6] M.H. Shaw, J. Twilton, D.W.C. MacMillan, Photoredox catalysis in organic chemistry, J. Org. Chem. 81 (2016) 6898–6926.
[7] R. Lindroth, K.L. Materna, L. Hammarström, C.-J. Wallentin, Sustainable Ir-photoredox catalysis by means of Heterogenization, ACS Org. Inorg. Au 2 (2022) 427, 423.
[8] S. Linic, P. Christopher, D.B. Ingram, Plasmonic-metal nanostructures for efficient conversion of solar to chemical energy, Nat. Mater. 10 (2011) 911–921.
[9] S. Mubeen, J. Lee, N. Singh, S. Krämer, G.D. Stucky, M. Moskovits, An Autonomous photosynthetic device in which all charge carriers derive from surface plasmons, Nat. Nanotechnol. 8 (2013) 247–251.
[10] X. Shi, K. Ueno, T. Oshikiri, Q. Sun, K. Sasaki, H. Misawa, Enhanced water splitting under modal strong coupling conditions, Nat. Nanotechnol. 13 (2018) 953–958.
[11] T. Oshikiri, K. Ueno, H. Misawa, Plasmon-induced ammonia synthesis through nitrogen photofixation with visible Light, Angew. Chem. Int. Ed. 53 (2014) 9802–9805.
[12] C. Wang, W.-C.D. Yang, D. Raciti, A. Bruma, R. Marx, A. Agrawal, R. Sharma, Endothermic reaction at room temperature enabled by deep-ultraviolet plasmons, Nat. Mater. 20 (2021) 346–352.
[13] H. Robatjazi, J.L. Bao, M. Zhang, L. Zhou, P. Christopher, E.A. Carter, P. Nordlander, N.J. Halas, Plasmon-driven carbon-fluorine (C(*sp3*)-F) bond activation with mechanistic insights into hot-carrier-mediated pathways, Nat. Catal. 3 (2020) 564–573.
[14] F.-X. Xiao, B. Liu, Plasmon-dicatated photo-electrochemical water splitting for solar-to-chemical energy conversion: current status and future perspectives, Adv. Mater. Interfac. 5 (2018), 1701098.
[15] K.-Y. Jiang, Y.L. Weng, S.-Y. Guo, Y. Yu, F.-X. Xiao, Self-assembly of metal-semiconductor via ligand engineering: unravelling the synergistic dual roles of metal nanocrystals toward plasmonic photoredox catalysis, Nanoscale 9 (2017) 16922–16936.
[16] Z. Zeng, T. Li, Y.-B. Li, X.-C. Dai, M.-H. Huang, Y. He, G. Xiao, F.-X. Xiao, Plasmon-induced photoelectrochemical water oxidation enabled by in situ layer-by-layer construction of cascade charge transfer channel in a multilayered photoanode, J. Mater. Chem. A 6 (2018) 24686–24692.
[17] C. Han, M.-.Y. Qi, Z.-R. Tang, J. Gong, Y.-J. Xu, Gold nanorods-based hybrids with tailored structures for photoredox catalysis: fundamental science, materials design and applications, Nano Today 27 (2019) 48–72.
[18] C. Han, S.-H. Li, Z.-R. Tang, Y.J. Xu, Tunable plasmonic core-shell heterostructures design for broadband light driven catalysis, Chem. Sci. 9 (2018) 8914–8922.
[19] N. Zhang, C. Han, X. Fu, Y.J. Xu, Funtion-oriented engineering of metal-based nanohybrids for photoredox catalysis: exerting plasmonic effect and beyond, Chem 4 (2018) 1832–1861.
[20] M.L. Brongersma, N.J. Halas, P. Nordlander, Plasmon-induced hot carrier science and technology, Nat. Nanotechnol. 10 (2015) 25–34.
[21] C. Zhan, J. Yi, S. Hu, X.-G. Zhang, W.-Y. Wu, Z.-Q. Tian, Plasmon-mediated chemical reactions, Nat. Rev. Methods Primers 3 (2023) 12.
[22] M.D. Levin, S. Kim, F.D. Toste, Photoredox catalysis unlocks single-electron Elementary steps in transition metal catalyzed Cross-coupling, ACS Cent. Sci. 2 (2016) 293–301.
[23] K. Goliszewska, K. Rybicka-Jasińska, J.A. Clark, V.I. Vullev, D. Gryko, Photoredox catalysis: the reaction mechanism can Adjust to electronic properties of a catalyst, ACS Catal. 10 (2020) 5920–5927.
[24] Y. Yang, L. Liu, W.-H. Fang, L. Shen, X. Chen, Theoretical Exploration of energy transfer and single electron transfer mechanisms to understand the generation of triplet Nitrene and the C(sp3)–H Amidation with photocatalysts, J. Am. Chem. Soc. Au 2 (2022) 2596–2606.
[25] Y. Sivan, I.W. Un, Y. Dubi, Assistance of metal nanoparticles in photocatalysis – nothing more than a classical heat source, Faraday Discuss 214 (2019) 215–233.
[26] G. Baffou, I. Bordacchini, A. Baldi, R. Quidant, Simple experimental procedures to distinguish phototehrmal from hot-carrier processes in plasmonics, Light Sci. Appl. 9 (2020) 108.
[27] R.A. Marcus, On the theory of oxidation-reduction reactions involving electron transfer. I, J. Chem. Phys. 24 (1956) 966.
[28] E. Sjulstok, J.M.H. Olse, I.A. Solov'yov, Quantifying electron transfer reactions in biological systems: what interactions play the major role? Sci. Rep. 5 (2016), 18446.
[29] M.K. Johnson, R.B. King, D.M. Kurts Jr, C. Kutal, M.L. Norton, R.A. Scott (Eds.), Electron Transfer in Biology and the Solid State, Advances in Chemistry, vol. 226, 1989.
[30] C.J. Grimes, D. Piszkiewicz, E.B. Fleischer, Electron transfer reactions in biological systems: the reduction of Ferricytochrome *c* by Chromous ions, Proc. Natl. Acad. Sci. USA 71 (1974) 1408–1412.
[31] S. Ma, R. Ludwig, Direct electron transfer of enzymes Facilitated by Cytochromes, Chemelectrochem 6 (2019) 958–975.
[32] Y. Anraku, Bacterial electron transport chains, Annu. Rev. Biochem. 57 (1988) 101–132.
[33] F. Kracke, I. Vassilev, J.O. Krömer, Microbial electron transport and energy conservation – the foundation for optimizing bioelectrochemical systems, Front. Microbiol. 6 (2015) 575.
[34] M.D. Kärkäs, E.V. Johnston, O. Verho, B. Åkermark, Artificial photosynthesis: from Nanosecond electron transfer to catalytic water oxidation, Acc. Chem. Res. 47 (2014) 100–111.
[35] L. Hammarström, S. Styring, Coupled electron transfers in artificial photosynthesis, Philos. Trans. R. Soc. Lond. B Biol. Sci. 363 (2008) 1283–1291.
[36] N. Kandoth, J.P. Hernádez, E. Palomares, J. Lloret-Filol, Mechanisms of photoredox catalysts: the role of optical spectroscopy, Sustain. Energy Fuels 5 (2021) 638–665.
[37] J. Piella, N.G. Bastús, V. Puntes, Size-controlled synthesis of Sub-10-nanometer citrate-Stabilized gold nanoparticles and related optical properties, Chem. Mater. 28 (2016) 1066–1075.
[38] M.P. Seah, G.C. Smith, M.T.A.E.S. Anthony, Energy calibration of electron spectrometers. I - an absolute, traceable energy calibration and the provision of atomic reference line energies, Surf. Interface Anal. 15 (1990) 293–308.
[39] N.H. Turner, A.M. Single, Determination of peak positions and areas from wide-scan XPS spectra, Surf. Interface Anal. 15 (1990) 215–222.
[40] L. Nan, J. Giráldez:Martínez, A. Stefancu, L. Zhu, M. Kiu, A.O. Govorov, L. V. Besteriro, E. Cortés, Investigating plasmonic catalysis kinetics on hot-Spot engineered Nanoantennae, Nano Lett. (2023), https://doi.org/10.1021/acs.nanolett.3c00219.

[41] V. Spampinato, M.A. Parracion, R. La Spina, F. Rossi, G. Ceccone, Surface analysis of gold nanoparticles functionalized with thiol-modified glucose SAMs for biosensor applications, Front. Chem. 4 (2016) 8.
[42] H.B. Lu, C.T. Campbell, D.G. Castner, Attachment of functionalized Poly(ethylene glycol) films to gold surfaces, Langmuir 16 (2000) 1611–1618.
[43] C. Vericat, M.G. Vela, G.A. Benitez, J.M. Martin Gago, X. Torrelles, R.C. Salvarezza, Surface characterization of sulfur and alkanethiolself-assembled monolayers on Au (111), J. Phys. Condens. Matter 18 (2006) R867–R900.
[44] J.A. Page, G. Wilkinson, The polarographic chemistry of ferrocene, ruthenocene and the metal hydrocarbon ions, J. Am. Chem. Soc. 74 (1952) 6149–6150.
[45] A. Paul, R. Borrelli, H. Bouyanfif, S. Gottis, F. Sauvage, Tunable redox potential, optical properties, and Enhanced stability of modified ferrocene-based complexes, ACS Omega 4 (2019) 14780–14789.
[46] H.G. Roth, N.A. Romero, D.A. Nicewicz, Experimental and calculated electrochemical potentials of common organic molecules for applications to single-electron redox chemistry, Synlett 27 (2016) 714–723.
[47] M. Maley, J.W. Hill, P. Saha, J.D. Walmsley, C.M. Hill, The role of Heating in the electrochemical response of plasmonic nanostructures under illumination, J. Phys. Chem. C 123 (2019) 12390–12399.
[48] A. Battacharjee, A. Rooj, D. Roy, M. Roy, Thermal Decomposition Study of ferrocene [$(C_5H_5)_2Fe$], J. Experim. Phys. 2014 (2014), 513268.
[49] S. Link, M.A. El-Sayed, Spectral properties and relaxation dynamics of surface plasmon electronic Oscillations in gold and Silver Nanodots and nanorods, J. Phys. Chem. B 103 (1999) 8410–8426.
[50] M. Valenti, A. Venupogal, D. Tordera, M.P. Jonsson, G. Biskos, A. Schmidt-Ott, W. A. Smith, Hot carrier generation and extraction of plasmonic Alloy nanoparticles, CAS Photon 4 (2017) 1146–1152.
[51] Y. Hattori, M. Abdellah, J. Meng, K. Zheng, J. Sá, Simultaneous hot electron and hole injection upon excitation of gold surface plasmon, J. Phys. Chem. Lett. 10 (2019) 3140–3146.
[52] Y. Hattori, S.G. Álvarez, J. Meng, K. Zheng, J. Sá, Role of the metal oxide electron acceptor on gold-plasmon hot-carrier dynamics and its implication to photocatalysis and photovoltaics, ACS Appl. Nano Mater. 4 (2021) 2052–2060.
[53] C. Bannwarth, S. Ehlert, S. Grimme, GFN2-xTB—an Accurate and broadly parametrized Self-consistent tight-binding quantum chemical method with multipole Electrostatics and density-Dependent Dispersion contributions, J. Chem. Theor. Comput. 15 (2019) 1652–1671.
[54] T.P. Rossi, T. Shegai, P. Erhart, T.J. Antosiewicz, Strong plasmon-molecule coupling at the nanoscale revealed by first-principles modeling, Nat. Commun. 10 (2019) 3336.
[55] G. Tagliabue, J.S. DuChene, M. Abdellah, A. Habib, D.J. Gosztola, Y. Hattori, W.-H. Cheng, K. Zheng, S.E. Canton, R. Sundararaman, J. Sá, H.A. Atwater, Ultrafast hot-hole injection modifies hot-electron dynamics in Au/p-GaN heterostructures, Nat. Mater. 19 (2020) 1312–1318.
[56] S.C. Bergmeier, The synthesis of Vicinal Amino Alcohols, Tetrahedron 56 (2000) 2561–2576.
[57] D. Nilov, O. Reiser, The Sharpless asymmetric aminohydroxylation –scope and limitation, Adv. Synth. Catal. 344 (2002) 1169–1173.
[58] J.A. Bodkin, M.D. McLeod, The Sharpless asymmetric aminohydroxylation, J. Chem. Soc. Perkin Trans. 1 (2002) 2733–2746.
[59] T.J. Donohoe, C.K.A. Callens, A. Flores, A.R. Lacy, A.H. Rathi, Recent Developments in methodology for the direct Oxyamination of Olefins, Chem. Eur J. 17 (2011) 58–76.
[60] F. Xu, L. Zhu, S. Zhu, X. Yan, H.C. Xu, Electrochemical intramolecular aminooxygenation of unactivated alkenes, Chem. Eur J. 20 (2014) 12740, 12544.
[61] M. Oestreic, G. Auer, Practical synthesis of Allylic Silanes from Allylic Esters and Carbamates by Stereoselective Copper-catalyzed Allylic Substitution reactions, Adv. Synth. Catal. 347 (2005) 637–640.
[62] M. Hatano, S. Kamiya, K. Moriyama, K. Ishihara, Lanthanum(III) Isopropoxide catalyzed Chemoselective transesterification of Dimethyl carbonate and methyl Carbamates, Org. Lett. 13 (2011) 430–433.